APL Photonics

RESEARCH ARTICLE | AUGUST 27 2025

Jitter in photon-number-resolved detection by superconducting nanowires

Mariia Sidorova ; Timon Schapeler ; Alexej D. Semenov ; Fabian Schlue ; Michael Stefszky ; Benjamin Brecht ; Christine Silberhorn ; Tim J. Bartley

APL Photonics 10, 086113 (2025)
https://doi.org/10.1063/5.0273752

Jitter in photon-number-resolved detection by superconducting nanowires

Cite as: APL Photon. 10, 086113 (2025); doi: 10.1063/5.0273752
Submitted: 1 April 2025 • Accepted: 6 August 2025 •
Published Online: 27 August 2025

Mariia Sidorova,[1,2,a] Timon Schapeler,[3,4] Alexej D. Semenov,[2] Fabian Schlue,[5] Michael Stefszky,[5] Benjamin Brecht,[5] Christine Silberhorn,[5] and Tim J. Bartley[3,4]

AFFILIATIONS

[1] Department of Physics, Humboldt-Universität zu Berlin, Newtonstr. 15, 12489 Berlin, Germany
[2] German Aerospace Center (DLR), Institute of Space Research, Rutherfordstr. 2, 12489 Berlin, Germany
[3] Department of Physics, Paderborn University, Warburger Str. 100, 33098 Paderborn, Germany
[4] Institute for Photonic Quantum Systems (PhoQS), Paderborn Unviersity, Warburger Str. 100, 33098 Paderborn, Germany
[5] Integrated Quantum Optics Group, Institute for Photonic Quantum Systems (PhoQS), Paderborn University, Warburger Str. 100, 33098 Paderborn, Germany

[a] **Author to whom correspondence should be addressed:** mariia.sidorova@ptb.de. **Present address:** Physikalisch-Technische Bundesanstalt (PTB), Abbestr. 2-12, 10587 Berlin, Germany.

ABSTRACT

By analyzing the physics of multi-photon absorption in superconducting nanowire single-photon detectors (SNSPDs), we identify physical components of jitter. From this, we formulate a quantitative physical model of the multi-photon detector response that combines the local detection mechanism and local fluctuations (hotspot formation and intrinsic jitter) with the thermoelectric dynamics of resistive domains. Our model provides an excellent description of the arrival-time histogram of a commercial SNSPD across several orders of magnitude, both in arrival-time probability and across mean photon number. This is achieved with just three fitting parameters: the scaling of the mean arrival time of voltage response pulses, as well as the Gaussian and exponential jitter components. Our findings have important implications for photon-number-resolving detector design, as well as applications requiring low jitter, such as light detection and ranging (LIDAR).

I. INTRODUCTION

Photon-number measurements are a cornerstone of experimental quantum optics and fundamental to our understanding of the quantized nature of light. They are used to measure photon statistics in order to classify quantum optical states[1] and perform projective measurements, which herald the presence of particular nonclassical photonic states.[2–5] Photon-number-resolved (PNR) measurements are also required for a broad range of applications in photonic quantum information processing, such as error identification in photonic quantum computing[6,7] and quantum key distribution.[8]

To measure photon number, one can rely on devices with an intrinsic photon-energy resolution. One archetypal example is the superconducting transition-edge sensor.[9,10] Nevertheless, these devices require significant millikelvin cryogenic overhead, and their timing characteristics (on the nano- to microsecond level) limit the range of experiments and applications. A more experimentally accessible alternative has been to use spatially and/or temporally multiplexed threshold detectors,[11–13] also called "on-off " or "click" detectors, such as single-photon avalanche photodiodes (SPADs) or superconducting nanowire single-photon detectors (SNSPDs). These detectors trigger on detecting at least one photon. By splitting an unknown number of photons into multiple modes, each of which is incident on its own detector, one can achieve quasi-photon-number resolution. This approaches perfect PNR when the number of detectors is much larger than the number of photons to be measured.[14,15]

SNSPDs are now well-established as the detector of choice for many experiments and applications of quantum optics and photonics because of their high efficiency, low noise, and accurate timing characteristics. SNSPDs were initially regarded as

threshold detectors. However, Cahall *et al.*[16] observed that some degree of photon-number information could be obtained by analyzing the electrical trace of the detector response, and since then a number of works have further refined this technique.[17–24] All of these rely on photons with an optical pulse duration shorter than the jitter of the detectors, typically below 100 ps. This is, however, well within the range of quantum light sources generated by nonlinearities.[25]

Schapeler *et al.*[22] showed that almost all photon-number information is contained within the rising edge of the electrical trace of the detector and that this is most accurately measured with a time-to-digital converter conditioned on a threshold. Central to extracting photon-number information is therefore the ability to measure this arrival time accurately, which requires an understanding of the underlying photon-number-dependent jitter mechanisms. However, while models for SNSPD jitter are well accepted,[26,27] the effects of photon number on jitter are far less well understood. Moreover, studying multi-photon absorption effects not only enhances our understanding of the underlying device physics of SNSPDs but also allows detectors to be designed to maximize this figure of merit, thereby unlocking further applications of this fundamental photonic technology.

In this paper, we present a physical model that accounts for the photon-number-dependent jitter of SNSPDs and apply it to experimental data obtained from a commercial device operated over a broad range of photon fluxes. We obtain excellent agreement between theory and experiment over several orders of magnitude in the arrival-time probability histogram. Based on this understanding, we suggest how SNSPDs can be designed to optimize their photon-number-resolving power.

II. SUPERCONDUCTING NANOWIRE DETECTOR PHYSICS AND JITTER MECHANISMS

Photon detection in superconducting nanowires involves sequential processes:[28] hotspot formation (vortex crossing in wide wires), resistive domain evolution, and electrical signal propagation. Each process introduces delays and variations that jointly determine the total jitter. The arrival-time histogram of voltage response pulses in single-photon detection with SNSPDs is well described with an exponentially modified Gaussian (EMG) distribution,[29]

$$P_{\mathrm{EMG}}(t,\sigma,\tau,\mu) = \frac{1}{2\tau}\exp\left(\frac{1}{2\tau}\left[\frac{\sigma^2}{\tau} - 2t + 2\mu\right]\right) \times \left[1 - \mathrm{erf}\left(\frac{\frac{\sigma^2}{\tau} - t + \mu}{\sigma\sqrt{2}}\right)\right], \quad (1)$$

where μ is the mean value and σ and τ are the Gaussian and exponential components, respectively.

For SNSPDs, the total measured jitter is typically determined as the histogram width, given by the standard deviation $\sigma_{\mathrm{tot}} = \sqrt{\sigma^2 + \tau^2}$. The Gaussian jitter component can be decomposed into its constituent contributions

$$\sigma = \sqrt{\sigma_{\mathrm{noise}}^2 + \sigma_{\mathrm{inst}}^2 + \sigma_{\mathrm{opt}}^2 + \sigma_{\mathrm{geom}}^2 + \sigma_{\mathrm{int}}^2}. \quad (2)$$

Among these, the first three components are due to external sources: noise in the electronics σ_{noise}, data acquisition instrumentation (e.g., time-to-digital converter, trigger photodiode) σ_{inst}, and optical pulse duration σ_{opt}. Geometric jitter σ_{geom} arises from the temporal uncertainty of where photons are absorbed along the wire, i.e., it is determined by the SNSPD geometry. The Gaussian σ_{int} together with exponential τ components constitute the jitter intrinsic to the photon detection process; throughout the paper, we refer to it as the intrinsic jitter ($\sqrt{\sigma_{\mathrm{int}}^2 + \tau^2}$).

Intrinsic jitter is determined by the physics of the hotspot formation process. It arises from thermal fluctuations affecting the detection energy barrier that dominate other jitter sources[30] like Fano fluctuations (phonon loss),[31] non-uniformities in the superconducting energy gap and variations in the film thickness,[32] local position-dependent threshold,[26] and vortex time-of-flight. In narrow nanowires, the vortex time-of-flight jitter is negligible (<1 ps).[33] Wider strips exhibit large vortex-induced jitter at low bias currents, but this diminishes at high currents, where vortex motion becomes fast and the position-dependent threshold flattens.[34] In this case, thermal fluctuations may again become the dominant jitter source.

After photon absorption, the hotspot region enters a metastable state with the free energy U defined by the photon energy and the actual local temperature, which itself is the subject of background thermal fluctuations in the absence of photons. Thermal fluctuations in the hotspot[30] (a Poisson stochastic process) may provide enough energy to escape the metastable state over the still remaining energy barrier ΔU (difference between the detection threshold and the actual energy). The escape rate (inverse of first hitting time[35]), distributed exponentially, varies with ΔU. For large ΔU, escapes are rare, producing an exponential tail in the arrival-time histogram parameterized by τ, while for smaller ΔU (e.g., in high-energy photon detection), escapes occur frequently, and the histogram retains the Gaussian shape inherent to the background fluctuations. The jitter in this case is defined by events driving the hotspot to energies above the detection threshold.[26]

The arrival-time histogram in multi-photon detection can be described using a sum of P_{EMG} [Eq. (1)] with different means μ corresponding to different photon numbers, each weighted by the probability for a given photon-number component in the underlying photon distribution P_n. For coherent light, this distribution is Poissonian with $P_n(\tilde{n}) = \frac{\tilde{n}^n e^{-\tilde{n}}}{n!}$, resulting in

$$P_{\mathrm{PNR}}(\tilde{n}) = \sum_{n=1}^{\infty} P_n(\tilde{n}) P_{\mathrm{EMG}}(t,\sigma_n,\tau_n,\mu_n), \quad (3)$$

for simplicity, uniform illumination is assumed. The key challenge in generalizing this model for multi-photon absorption is therefore to account for photon-number dependence in each of the parameters in the P_{EMG} distribution, the jitter components, and μ_n. The photon-number dependence of μ_n has previously been studied by Nicolich *et al.*[36] Here, we refine this model and discuss additionally the photon-number dependence of σ and τ arising from multi-photon absorption.

To do this, we first consider the underlying physics of different multi-photon absorption scenarios.

A. Multi-photon absorption at the same site

When multiple photons n, each of energy $h\nu$, are absorbed simultaneously within the hotspot size, the deposited energy is

$E = n \cdot h\nu$ [see Fig. 1(a-i)]. Higher energy deposition leads to a shorter intrinsic delay, as this is proportional to $1/(E - E_0)$ due to the energy-dependent collapse time of the superconducting order parameter (E_0 is the photon energy corresponding to the detection threshold[26,27,37]), depicted in Fig. 1(a-iii). Furthermore, for the same dispersion in the background energy fluctuations, intrinsic jitter decreases with n. Hence, for $E > E_0$, increasing n results in earlier domain growth and, therefore, earlier voltage response pulse arrivals μ (alongside reduced intrinsic jitter, akin to detecting a higher energy photon[38]). Note, this does not affect the dynamics of the resistive domain (i.e., rise time t_{rise}) but only the delay μ and the intrinsic jitter [see Fig. 1(a-ii)]. Despite the fact that for $E < E_0$ the detection mechanism is different and is governed by fluctuations,[30] the qualitative result remains, i.e., intrinsic jitter decreases as n increases.

Given the small characteristic hotspot size ($L_T \approx 50$ nm in NbTiN[39] and $L_T \approx 220$ nm in WSi[40]), the probability of multi-photon absorption at the same site is higher in detectors with smaller active areas, such as those integrated with waveguides[41] or nanodetectors.[42] If the area does not exceed the hotspot size, the intrinsic jitter monotonously decreases as both the number of photons and the mean photon number (light intensity) increase.

For detectors with areas exceeding the hotspot size, there are several independent absorption sites (bins) over which incident photons are distributed randomly. This results in a combination of measurement events in which multiple photons are absorbed at the same site or independently at different sites.

B. Simultaneous multi-photon absorption at independent sites

When non-overlapping (independent) resistive domains [see Fig. 1(b)] are created, they share the same transport current, which correlates their dynamics. As the number of domains increases, the wire resistance R grows faster, causing the current to divert more rapidly into the external circuit and producing a voltage response pulse with a shorter rising time $t_{\text{rise}} = L_k/R \propto 1/\sqrt{n}$ [see Fig. 1(b)]. This is because $R \propto ntu$, where u is the domain wall propagation rate, and the voltage rise $V(t) \propto (1 - e^{-t^2 nu})$ reaches $(1 - e^{-1})$ when $t \propto 1/\sqrt{n}$ (which holds for linear slopes near the 50% pulse amplitude). This results in photon-number dependent mean arrival times $\mu_n \propto 1/\sqrt{n}$, as shown by Nicolich *et al.*[36] The non-linear electrothermal model[43] refines this to $t_{\text{rise}} \propto n^{-\alpha}$, where $\alpha \in [0.3, 0.4]$ due to the current-dependence of the domain wall propagation rate, in agreement with experimental results.[23]

C. Delayed multi-photon absorption at independent sites

When photons are absorbed at independent sites with a time delay, typically due to optical pulse durations σ_{opt} longer than the hotspot formation time (about the electron–phonon cooling time), the detection process becomes more complex. The first photon creates a hotspot and a growing resistive domain, causing the current to start diverting into the external circuit. The second photon, absorbed at a different site, encounters a reduced current. At smaller currents, the remaining energy barrier is larger, leading to even later emergence of the second domain, larger intrinsic jitter, and reduced detection efficiency (if not saturated). Under the reduced current, domain growth is slower, so that when the first domain has already disappeared, the second domain may still exist. This increases the voltage rise time compared to the case of simultaneous photon absorption, affecting not only intrinsic jitter but also the mean of a distribution. The resolvable delay between photons is determined by how long the current persists in the detector above the level at which the detection efficiency remains equal to the steady-state saturated value. This timescale is set either by the circuit time constant (in long, high-inductance, or shunted wires) or by the electron–phonon cooling time (in short, low-inductance wires).

D. Impact of resistive domain overlap

Overlapping domains compromise photon-number resolution, as two photons absorbed within the domain length are detected

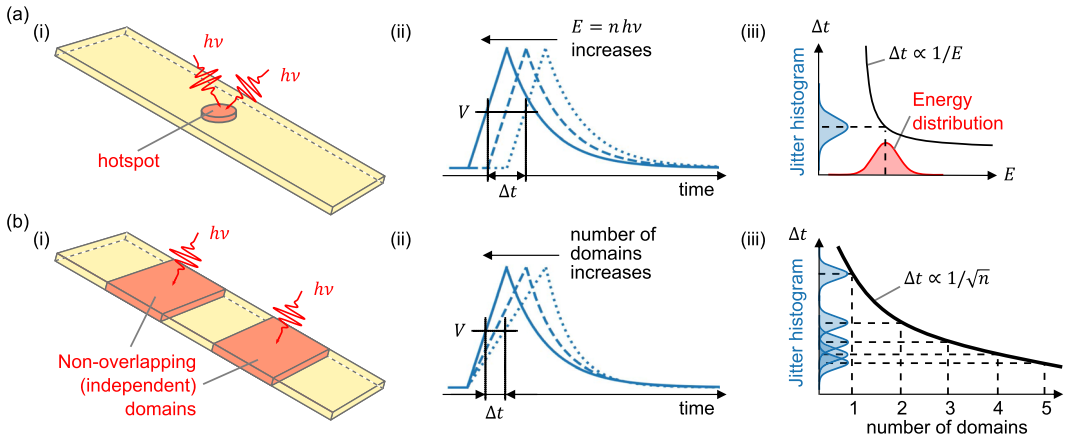

FIG. 1. Jitter in different scenarios of multi-photon detection in superconducting strips. (a) (i) Upon multi-photon absorption at the same site (within a hotspot), the deposited energy $E = n \cdot h\nu$ scales with the number of absorbed photons n, each of energy $h\nu$. (ii) Arrival time decreases as E increases. (iii) Higher energy reduces the intrinsic delay time and narrows the jitter distribution. (b) (i) When multiple photons induce n independent hotspots and each generates a non-overlapping resistive domain, (ii) the slope of the voltage response pulse becomes faster $\propto 1/\sqrt{n}$. (iii) The corresponding arrival-time histogram as a function of photon number.

as one. For a nanowire composed of M independent bins, each of the domain length, the probability that no bin contains more than one photon ($n \le M$, photons are uniformly distributed) is $P(\text{no overlap}) = \prod_{i=0}^{n-1} \frac{M-i}{M}$. This arises because the first photon can occupy any of the M bins with probability $1/M$, the second photon avoids the already-occupied bin with probability $(M-1)/M$, and so on. Then the probability that at least one bin contains two photons is

$$P(\text{overlap}) = 1 - \prod_{i=0}^{n-1} \frac{M-i}{M} \approx 1 - \exp\left(-\frac{n(n-1)}{2M}\right), \quad (4)$$

the approximation is valid for $n \ll M$.

This is a special case of the inclusion–exclusion principle for the probability that k from n photons generate independent non-overlapped domains[11]

$$P_{\mathrm{M}}(k|n) = \frac{1}{M^n} \frac{M!}{k!(M-k)!} \sum_{j=0}^{k} (-1)^j \frac{k!}{j!(k-j)!} (k-j)^n, \quad (5)$$

for $k \le n \le M$. For $k = n$, i.e., no overlap at all, one gets $P_{\mathrm{M}}(n|n) = M!/[(M-n)!M^n] = P(\text{no overlap})$.

The probability given by Eq. (5) can be added to the PNR model [under the sum in Eq. (3)] to correct for overlap (see discussion in Sec. IV A). Note, the overlap probability is never zero.

E. Multi-photon geometric jitter

Geometric jitter σ_{geom} arises from spatial variations in the propagation time of the electrical signal from the photon absorption position x to the readout electronics. If the nanowire can be treated as a transmission line (which may not hold under all circumstances[44]), two electrical pulses propagate with velocity v toward either end of the nanowire with length l. In the differential readout scheme,[45,46] the absolute arrival time difference at the readout is $\Delta t = |x/v - (l-x)/v| = 2x/v$. For uniform illumination and single-photon detection, the time difference $\Delta t/2 = x/v$ is also uniformly distributed, resulting in position-dependent uncertainty, i.e., geometric jitter. The corresponding geometric jitter is $\sigma_{\text{geom},1} = l/(2\sqrt{3}v)$, which yields ≈ 5 ps per 100 μm of nanowire length (for typical v = 6 μm/ps[45,46]).

For two-photon detection, the distribution of the time difference Δt follows a symmetric triangular distribution because at least one site is more likely to be closer to the nanowire ends [see orange bars in Fig. 2(a)]. The geometric jitter for this case, $\sigma_{\text{geom},2} = l/(2\sqrt{6}v)$, is reduced by a factor of $\sqrt{2}$ compared to single-photon detection. For three-photon detection, the time difference Δt is determined by the two outermost absorption sites. Since one site always falls between the other two, the variation of Δt is constrained, leading to a narrower, more peaked distribution than the triangular case for two sites [see Fig. 2(a)]. Geometric jitter therefore decreases as the photon-number state increases, following $\sigma_{\text{geom},n} \propto n^{-0.75}$ (with the exponent determined numerically by Monte-Carlo simulations).

The time-difference distribution was experimentally observed in Ref. 46 [see Fig. 3(a) therein] for different pulsed light intensities. It represents a convolution of distributions corresponding to single- and multi-photon events weighted by the Poisson probabilities of the photon number, although this interpretation was not recognized at the time.

Now consider a conventional readout scheme, where one end of the nanowire is shorted to the ground. At the absorption site x, one electrical pulse propagates directly to the readout end, and the other first reaches the shorted end and then, propagating through the ground, arrives at the readout end. The arrival time of the "center of mass" $\Delta t = |t_1 + t_2|/2 = (l/v + l/v_g)/2$ is independent of position and, therefore, does not cause geometric jitter unless the dispersion and losses differ between the nanowire and the ground plane.[29] Here, $v_g \approx 140$ μm/ps is the propagation velocity through the ground plane; since $v_g \gg v$, the contribution of the last term l/v_g is negligible. Alternatively (depending on the device layout and circuit implementation), the second pulse can be reflected by the ground and propagate back toward the readout through the nanowire itself. In this scenario, the geometric jitter can be canceled at a specific voltage trigger.[47]

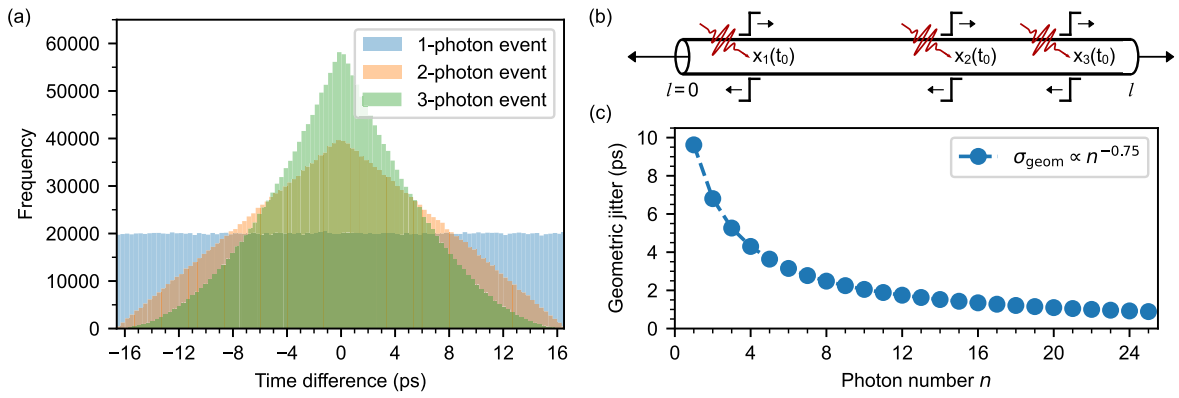

FIG. 2. (a) Distributions of time differences Δt for one-, two-, and three-photon events show flat, triangular, and peaked shapes, respectively. (b) Schematic showing the origin of geometric jitter. (c) Geometric jitter σ_{geom} as a function of photon number n.

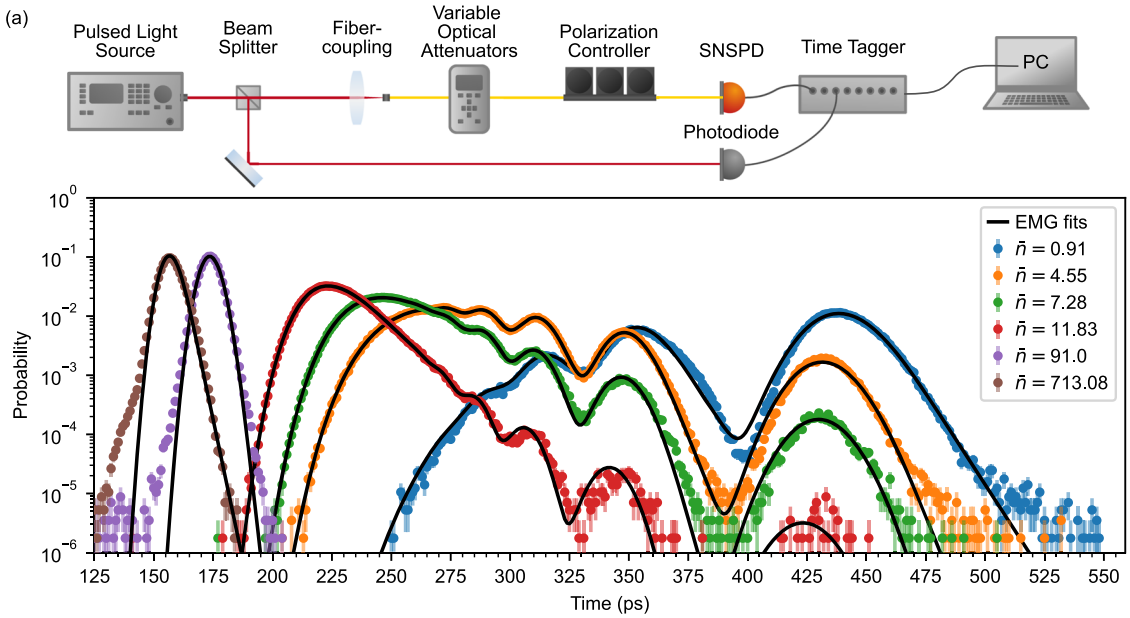

FIG. 3. (a) Experimental setup to measure photon-number resolution with SNSPDs based on the rising edge arrival times relative to a trigger signal. Refer to the main text for more details. (b) Arrival-time histograms for different mean photon numbers $\bar{n}$ specified in the legend (the error bars are based on Poisson errors of the counting statistics). The black lines correspond to the best fits based on a sum of exponentially modified Gaussian distributions [Eq. (3)].

III. COMPARISON TO EXPERIMENT

We characterize the PNR response of a commercial SNSPD (Single Quantum, 2023) made of a 1.4 mm-long, 70 nm-wide, meandered NbTiN nanowire with 140 nm pitch at an operating temperature of 2.3 K (the sheet resistance and transition temperature were not disclosed). The detector is operated at a bias current of 17.7 μA with a switching current of 19.3 μA as specified by the manufacturer; it achieves a system detection efficiency of $(91 \pm 3)\%$ with 19 ps jitter (FWHM, or 8 ps std; we assume that this was obtained at $\bar{n} \ll 1$ with a short pulsed laser). The single-ended readout chain, designed by the manufacturer (the circuit was not disclosed), includes cryogenic amplifiers with a 1 GHz bandwidth.

From the recorded electrical traces, we extract the following parameters: the detector dead time of ≈150 ns defined as the time at which the voltage signal drops below the noise level; the root-mean-square baseline noise $\sigma_{\mathrm{elec}} = 4.9$ mV; the 20%–80% voltage rise time in response to a single photon $t_{\mathrm{rise},1} = 0.68$ ns, and the corresponding slew rate $\gamma_{\mathrm{slew},1} = \mathrm{d}A/\mathrm{d}t = 1.08$ mV ps^{-1} (which holds for linear slopes near 50% of the pulse amplitude A). Using these values, we estimate the noise jitter as $\sigma_{\mathrm{noise}} = \sigma_{\mathrm{elec}}/\gamma_{\mathrm{slew}} = 4.5$ ps.

The experimental setup, Fig. 3(a), comprises a 1550 nm pulsed light source with 2.4 ps pulse duration (FWHM, $\sigma_{\mathrm{opt}} = 1$ ps std) at a 9.5 kHz repetition rate, which was reduced from 80 MHz using a pulse picker. Two variable optical attenuators accurately set the mean photon number per optical pulse (with uncertainty ±5%, see Ref. 22). Manual fiber polarization controllers are used to maximize the SNSPD count rate. The arrival times of SNSPD signals are recorded using a Time Tagger X (Swabian Instruments, < 2 ps std jitter) triggered by the fast photodiode (5 GHz bandwidth). The time tagger threshold is set at half the peak amplitude of the SNSPD signal for optimal photon-number resolution.[22] We acquired 122 datasets spanning mean photon numbers from 1 to ~68 000 photons per pulse, with 570 000 events recorded for each set. Figure 3(b) shows six representative experimental datasets for different mean photon numbers per optical pulse $\bar{n}$ (colored dots).

We describe the arrival-time histograms with our PNR model [Eq. (3)], making the following assumptions: (i) as an ansatz, we assume the intrinsic jitter components, σ_{int} and τ, do not depend on the photon number n, but we allow them to vary with the mean photon number $\bar{n}$ (see the beginning of the discussion in Sec. IV); (ii) we disregard time-walk artifacts,[48] arising from count rate dependent variations in the bias current, due to the long optical pulse period (105 μs) compared to the SNSPD dead time (150 ns); (iii) we empirically allow the one-photon peak position μ_1 to vary with photon flux to account for unknown circuit effects (e.g., ringing, bandwidth); (iv) we neglect delayed photon absorption effects despite the optical pulse duration (2.4 ps FWHM) being comparable to the hotspot formation time in NbTiN (≈5 ps).

Under these assumptions, the photon-number-dependent model parameters are

$$\mu_n \to \mu_\infty + \frac{\mu_1 - \mu_\infty}{\sqrt{n}} \propto \frac{t_{\mathrm{rise},1}}{\sqrt{n}}, \tag{6a}$$

$$\sigma_{\mathrm{noise},n} \to \frac{\sigma_{\mathrm{elec}}}{\gamma_{\mathrm{slew},1}\sqrt{n}} \approx \frac{\sigma_{\mathrm{elec}} t_{\mathrm{rise},1}}{A\sqrt{n}}, \tag{6b}$$

$$\sigma_{\mathrm{geom},n} \to \frac{\sigma_{\mathrm{geom},1}}{n^{0.75}}, \tag{6c}$$

and the remaining parameters are instrumental jitter σ_{inst} = 3 ps (from time-tagger and trigger photodiode), optical jitter σ_{opt} = 1 ps, and intrinsic jitter τ and σ_{int}. In Eq. (6a), μ_∞ = 144 ps is an arbitrary offset delay in our setup (the time difference between the trigger signal and the steepest rising edge). In Eq. (6c), the one-photon geometric jitter $\sigma_{geom,1}$ = 9 ps was pre-fitted and held constant across all datasets while the exponent 0.75 was determined numerically (see Sec. II E). The three primary fitting parameters are μ_1, τ, and σ_{int}.

As shown in Fig. 3(b) (black curves), the model is in excellent agreement over several orders of magnitude of the arrival-time probability and across a wide range of $\bar{n}$ from 1 to 500 per optical pulse.

To cover a wider range of fluxes $\bar{n}$ from 0.001 to 1000 and validate the model robustness, we performed additional arrival-time measurements (see Fig. 5 in Appendix) with a laser diode with a 10 kHz repetition rate and a larger pulse duration of σ_{opt} = 4 ps (std). The datasets with both light sources are well described by the model.

Figure 4(a) (red and green colored symbols) shows how the total width of the arrival-time histogram depends on the photon flux (similar experimental data were obtained from a waveguide-integrated SNSPD[49]). In the limit of large photon fluxes, the SNSPD jitter diminishes, which has been addressed in Ref. 37, attributed to the bolometric regime, i.e., when the total deposited photon energy turns a large section of the wire normal.

In Figs. 4(b) and 4(c), we show the best-fit values of the intrinsic jitter $\sqrt{\sigma_{int}^2 + \tau^2}$ and the one-photon peak position μ_1 obtained when describing the experimental histograms partly shown in Fig. 3(b) and in Fig. 5. As expected, in the few-photon range $\bar{n} \ll 1$, the intrinsic jitter stays broadly constant, while it decreases at high photon flux due to overlap and heating effects. The one-photon peak position μ_1 shows inconsistent behavior. For the data acquired with a pulse-picked system, μ_1 shifts toward earlier times, likely due to residual unpicked pulses causing detector heating (this agrees with electrothermal simulations), while for diode laser measurements, μ_1 shifts toward later times and then decreases.

We took a closer look at this discrepancy by changing the diode laser repetition rate from 1 kHz to 1 MHz (see Fig. 5 in the Appendix); however, we leave these effects outside the scope of this work, as they do not impact our main conclusions regarding jitter mechanisms.

IV. DISCUSSION

While it is clear that our results agree with the PNR model very well, we made a number of assumptions that may not be applicable in all uses.

First, while circuit-related effects (finite bandwidth, over-/undershoot in current, etc.) remain uncharacterized in our setup, they likely influence the observed shifts in the one-photon peak position in Figs. 4(b) and 4(c).

Second, as expected, the total jitter at high photon fluxes $\bar{n} > 100$ drops below that at low fluxes $\bar{n} \ll 1$ [see Fig. 4(a)] as its components due to noise, geometry, and intrinsic physics diminish. However, the reduction in intrinsic jitter [Figs. 4(b) and 4(c)] appears at a much smaller $\bar{n} \approx 10$ than anticipated. We estimate that our nanowire comprises ~10^3 independent *domain* detection bins (from our simulations, the domain length scales as 2 μm/$\sqrt{n}$) and ~10^4 independent *hotspot* detection bins (with hotspot size $L_T \approx 50$ nm in NbTiN), suggesting that overlap effects should only become relevant at $\bar{n} > 10^2$. We attribute this premature reduction in jitter to the limited bandwidth of our readout electronics (BW = 1 GHz), which distorts rising edges of voltage pulses generated by photon numbers $n > 4$ ($t_{rise} = 0.35/BW$). This limited bandwidth may also shift the one-photon peak position μ_1.

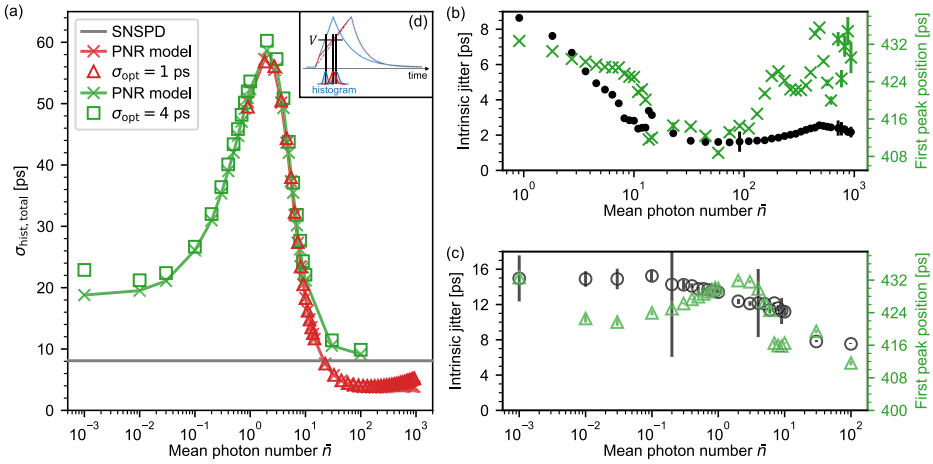

FIG. 4. (a) Total width of the arrival-time histogram $\sigma_{hist,total}$ as a function of mean photon number for datasets taken with two light sources with different optical jitter (as indicated in the legend). The model and experiment show close agreement. The gray line corresponds to the reference SNSPD jitter of 8 ps (std, as specified by the manufacturer). (b) Best-fit intrinsic jitter $\sqrt{\sigma_{int}^2 + \tau^2}$ (left, black axis) and the mean position μ_1 (right, green axis) of the one-photon histogram peak from Eq. (1), for the dataset with optical jitter of σ_{opt} = 1 ps. The error bars are based on the fitting uncertainty. (c) Best-fit parameters for the dataset with optical jitter of σ_{opt} = 4 ps. The arrival-time histograms and fits are shown in Fig. 5(b). The inset (d) shows a schematic of voltage response pulses from a single domain (blue dashed line), two independent domains (blue solid line). and initially two independent domains that then merge into each other (red solid line).

In scenarios of multi-photon absorption at independent sites, intrinsic jitter is influenced by the photon number due to the following: each absorbed photon initiates a delay in the emergence of a resistive domain, according to the local fluctuations, which are not correlated. The shortest delay determines the voltage pulse arrival time, similar to the effect of delayed multi-photon absorption described in Sec. II C. As the number of photons increases, the intrinsic jitter decreases for the same reason as for multi-photon geometric jitter in Sec. II E. Statistical analysis showed that for the studied detector this effect is small and can be neglected.

A. Limitations due to overlap

Although our primary analysis neglects domain overlap, Eq. (5) provides a first-order correction that accounts for it. This leads to a positive skew in the arrival-time distribution (underestimation of high photon-number events and overestimation of low photon-number events). Increasing the nanowire length reduces the overlap probability, while adding a series inductance or a shunt resistance has the opposite effect; it slows down the current dynamics and effectively increases the domain size, thereby increasing the overlap probability.

The situation is different when domains merge while growing, which is not described by Eq. (5). Electrothermal simulations[50] show that in such cases, the voltage response initially follows the two-domain dynamics but transitions to one-domain behavior as domains merge [see Fig. 4(d) for a schematic]. These events populate earlier times in the first peak, shifting its mean value to earlier times as $\bar{n}$ increases. This process is of a continuous nature, as the distance between two initially non-overlapping domains varies continuously. Therefore, the time at which the domains grow into each other and the voltage transitions to the one-domain dynamics is also continuous.

Hotspot overlap becomes significant only at higher fluxes $\bar{n}$ due to their smaller size compared to the domain. While hotspot overlap does not affect the rise time, it reduces the arrival time, populating earlier times in the histogram [see Fig. 1(a-ii)]. For SNSPDs operating below detection efficiency saturation, this can result in overestimation of high photon-number states.

B. Implications for detector engineering

First of all, this PNR method can only work for optical pulse durations σ_{opt} below characteristic timescales determined by the detector material and circuit. This limit is set either by hotspot formation time [typically about the electron–phonon cooling time, ≈5 ps in NbTiN,[39] ≈15 ps in WSi,[39] and ≈12 – 20 ps in MoSi (unpublished)] or, in SNSPDs with saturated detection efficiency, by the time during which the current in the nanowire remains above the level with saturated efficiency. In devices with no saturation, PNR signatures may still be resolvable for longer optical pulses, though with reduced efficiency and increased jitter, either up to the resistive domain lifetime [≈50 ps[51] in NbTiN, ≈630 ps in WSi,[52] and ≈70 – 130 ps in MoSi (unpublished)] or up to the time the current remains in the detector (Sec. II C).

Optimizing PNR efficiency, i.e., distinguishability of different photon numbers, requires maximizing the separation between the one-photon and the many-photon (steepest) voltage pulse $(\mu_1 - \mu_\infty)$ while minimizing all the jitter contributions. From Eq. (6a), maximizing $(\mu_1 - \mu_\infty)$ means increasing the rise time $t_{\mathrm{rise},1}$. One approach is increasing the wire length and, therefore, the kinetic inductance L_k, since $t_{\mathrm{rise}} \propto L_k$, which also helps to suppress domain overlap, albeit at the cost of increased geometric jitter and increased detector's dead time $t_{\mathrm{dead}} = t_{\mathrm{fall}} \log(N/A)$, where N is the noise level and $t_{\mathrm{fall}} = L_k/50\ \Omega$ is the voltage falling time. These trade-offs must be carefully considered when optimizing the detector's design for PNR, as has been noted in Refs. 23 and 41.

Longer rise times relax the bandwidth requirements, which must satisfy $\mathrm{BW} = 0.35\sqrt{n}/t_{\mathrm{rise},1}$ to avoid pulse distortion. However, the variance due to noise increases proportionally [Eq. (6b)]. Reducing the electrical noise by using low-noise cryogenic amplifiers has become a well-established technique in the community, therefore enhancing PNR (which has also been noted in Ref. 24). Furthermore, increasing the voltage pulse amplitude, which means maximizing the bias current, can also help. The combination of large bias currents and large area detectors is readily achieved by using micron-wide wires.[53–55] With this approach, Kong *et al.*[23] achieved PNR up to ten photons, sacrificing the reset time.

It is also apparent from Eqs. (6b) and (6c) that noise and geometric jitter can be effectively removed when using a large number of photons per pulse due to the inverse proportionality on n. This has practical implications in laser ranging: higher photon fluxes improve resolution, as multi-photon events reduce the timing jitter (also the intrinsic jitter due to overlap effects) and sharpen the histogram peak.[56] This was observed in very early work on SNSPDs.[57]

Finally, in real-world quantum photonics applications, single-photon sources typically used emit photons with durations ranging from 100 ps to a few nanoseconds, which SNSPDs must be able to handle for optimal PNR in such settings.

V. CONCLUSION

In this work, we have provided a quantitative model of photon-number dependent traces of SNSPDs, which includes both the arrival time and photon-number dependent jitter. Our model accurately predicts the arrival-time probability histogram across several orders of magnitude for a broad range of mean numbers of incident photons. Implementation of the model will enable the design of detectors with maximized PNR capability. While these results are certainly promising, there are additional effects that can be incorporated into future modeling, such as double-ended or differential read-out of the SNSPDs (eliminating geometric jitter) or the use of impedance matching tapers.[58]

ACKNOWLEDGMENTS

Partially funded by the European Union (ERC, QuESADILLA, 101042399). The views and opinions expressed are, however, those of the author(s) only and do not necessarily reflect those of the European Union or the European Research Council Executive Agency. Neither the European Union nor the granting authority can be held responsible for them. This work has received funding from the German Ministry of Education and Research within the PhoQuant project (Grant No. 13N16103). F.S. is part of the Max Planck School of Photonics, supported by the German Federal Ministry of Education and Research (BMBF), the Max Planck Society, and the Fraunhofer Society.

The identification of any manufacturer or supplier in this work shall not be taken as an endorsement or recommendation of specific products provided by the said manufacturer.

AUTHOR DECLARATIONS

Conflict of Interest

The authors have no conflicts to disclose.

Author Contributions

Mariia Sidorova: Conceptualization (lead); Formal analysis (equal); Investigation (equal); Methodology (equal); Software (equal); Validation (supporting); Visualization (supporting); Writing – original draft (equal); Writing – review & editing (equal). **Timon Schapeler**: Conceptualization (supporting); Data curation (lead); Formal analysis (equal); Investigation (equal); Methodology (equal); Software (equal); Visualization (lead); Writing – original draft (equal); Writing – review & editing (equal). **Alexej D. Semenov**: Conceptualization (supporting); Formal analysis (equal); Methodology (equal); Validation (lead); Writing – review & editing (equal). **Fabian Schlue**: Data curation (supporting); Investigation (equal); Writing – review & editing (equal). **Michael Stefszky**: Data curation (supporting); Funding acquisition (supporting); Project administration (equal); Supervision (equal); Writing – review & editing (equal). **Benjamin Brecht**: Data curation (supporting); Funding acquisition (supporting); Project administration (equal); Supervision (equal); Writing – review & editing (equal). **Christine Silberhorn**: Funding acquisition (equal); Project administration (equal); Resources (equal); Supervision (equal); Writing – review & editing (equal). **Tim J. Bartley**: Funding acquisition (equal); Project administration (equal); Resources (equal); Supervision (equal); Writing – original draft (equal); Writing – review & editing (equal).

DATA AVAILABILITY

The data that support the findings of this study are openly available in Zenodo at https://doi.org/10.5281/zenodo.14888684.

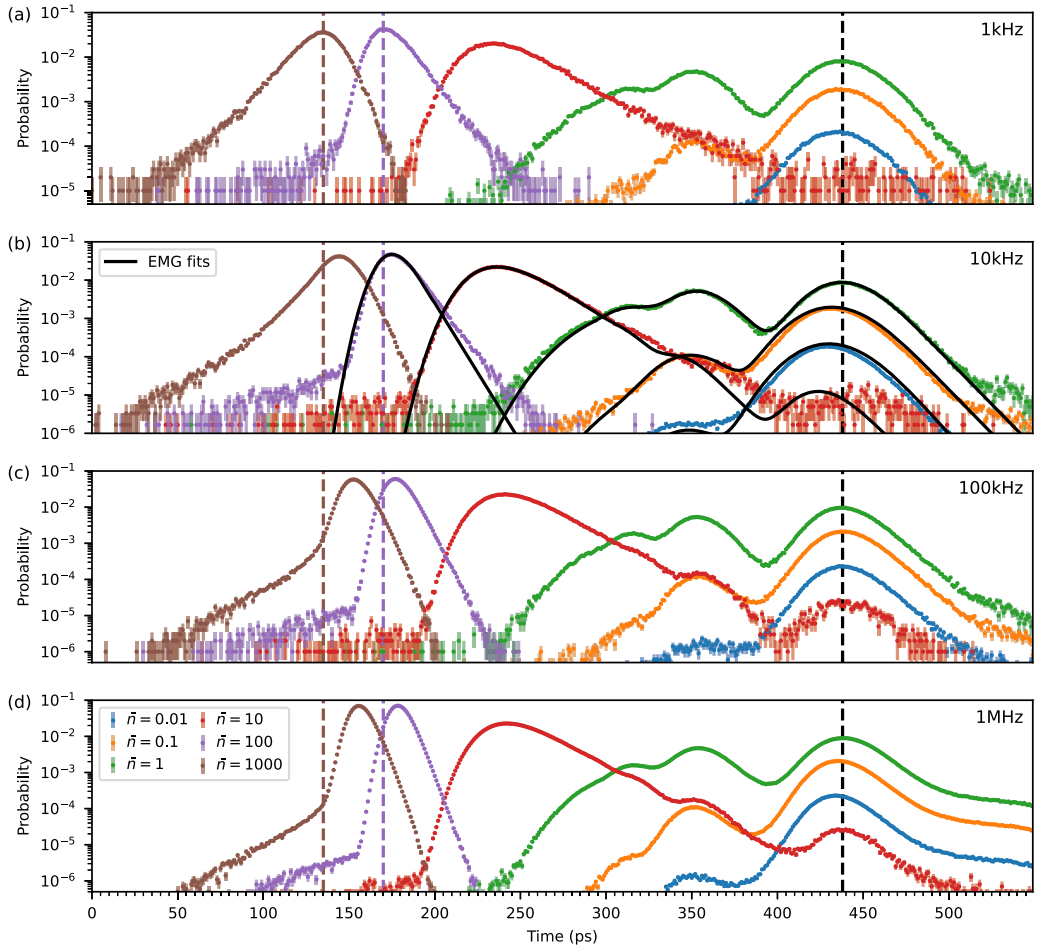

FIG. 5. Arrival-time probabilities measured at fixed laser repetition rates of (a) 1 kHz, (b) 10 kHz, (c) 100 kHz, and (d) 1 MHz. The shared legend shows the mean photon number per optical pulse (the error bars are based on Poisson errors of the counting statistics). The black lines in (b) for a 10 kHz repetition rate show the best fits with Eq. (3); the best fit parameters are plotted in Fig. 4(c).

APPENDIX A: ARRIVAL-TIME PROBABILITIES AT DIFFERENT PULSE REPETITION RATES

Here, we present arrival-time histograms measured with an alternative light source: a diode laser emitting at 1556 nm wavelength, with a pulse duration of 9.0 ps (FWHM, 3.8 ps std). We varied the laser pulse repetition rate from 1 kHz to 1 MHz and the mean photon number per pulse from 0.01 to 1000 (see Fig. 5). For reference, the detector dead time is ~150 ns (≈ 7 MHz).

Histograms obtained at 10 kHz were described with our PNR model; the best-fit parameters are shown in Fig. 4(c). The extracted intrinsic jitter is larger, which we attribute to the longer optical pulse duration exceeding the hotspot formation time in NbTiN (~5 ps). This means we are operating in the regime closer to the delayed photon absorption rather than the simultaneous photon absorption.

The data in Fig. 5 show two trends: (i) at large mean photon numbers ($\bar{n}$ = 1000, brown points in Fig. 5), where the detector operates in the bolometric regime, a large part of the wire becomes normal, and the histogram shifts systematically toward longer arrival times as the repetition rate increases (e.g., 135 ps at 1 kHz vs 156 ps at 1 MHz); and (ii) the one-photon peak also slightly shifts to later arrival times (for $\bar{n}$ increasing from 0.01 to 1, the shift is 2.5 ps at 1 kHz and 5 ps at 1 MHz). We also note that the width of the one-photon histogram peak increases at lower repetition rates, likely due to Allan variance over long measurement times.

Since neither the specific circuit design nor the thermal coupling of the commercial detector is known, we leave the interpretation of these behaviors outside the scope of this work. However, we note that one may disregard the effect of heating because electrothermal simulations show that for fixed bias current, increasing the bath temperature in contrast leads to earlier arrival times. One may also exclude current over- and undershooting because the laser repetition rate remains much below the detector's inverse dead time of 7 MHz.

REFERENCES

[1] L. Mandel, "Sub-Poissonian photon statistics in resonance fluorescence," Opt. Lett. **4**, 205 (1979).

[2] C. K. Hong and L. Mandel, "Experimental realization of a localized one-photon state," Phys. Rev. Lett. **56**, 58 (1986).

[3] M. Cooper, L. J. Wright, C. Söller, and B. J. Smith, "Experimental generation of multi-photon Fock states," Opt. Express **21**, 5309 (2013).

[4] J. Tiedau, T. J. Bartley, G. Harder, A. E. Lita, S. W. Nam, T. Gerrits, and C. Silberhorn, "Scalability of parametric down-conversion for generating higher-order Fock states," Phys. Rev. A **100**, 041802 (2019).

[5] M. Endo, R. He, T. Sonoyama, K. Takahashi, T. Kashiwazaki, T. Umeki, S. Takasu, K. Hattori, D. Fukuda, K. Fukui, K. Takase, W. Asavanant, P. Marek, R. Filip, and A. Furusawa, "Non-Gaussian quantum state generation by multi-photon subtraction at the telecommunication wavelength," Opt. Express **31**, 12865 (2023).

[6] P. Kok, W. J. Munro, K. Nemoto, T. C. Ralph, J. P. Dowling, and G. J. Milburn, "Linear optical quantum computing with photonic qubits," Rev. Mod. Phys. **79**, 135 (2007).

[7] I. Walmsley, "Light in quantum computing and simulation: Perspective," Opt. Quantum **1**, 35 (2023).

[8] N. Gisin, G. Ribordy, W. Tittel, and H. Zbinden, "Quantum cryptography," Rev. Mod. Phys. **74**, 145 (2002).

[9] A. E. Lita, A. J. Miller, and S. W. Nam, "Counting near-infrared single-photons with 95% efficiency," Opt. Express **16**, 3032 (2008).

[10] M. von Helversen, J. Böhm, M. Schmidt, M. Gschrey, J.-H. Schulze, A. Strittmatter, S. Rodt, J. Beyer, T. Heindel, and S. Reitzenstein, "Quantum metrology of solid-state single-photon sources using photon-number-resolving detectors," New J. Phys. **21**, 035007 (2019).

[11] H. Paul, P. Törmä, T. Kiss, and I. Jex, "Photon chopping: New way to measure the quantum state of light," Phys. Rev. Lett. **76**, 2464 (1996).

[12] M. J. Fitch, B. C. Jacobs, T. B. Pittman, and J. D. Franson, "Photon-number resolution using time-multiplexed single-photon detectors," Phys. Rev. A **68**, 043814 (2003).

[13] D. Achilles, C. Silberhorn, C. Śliwa, K. Banaszek, and I. A. Walmsley, "Fiber-assisted detection with photon number resolution," Opt. Lett. **28**, 2387 (2003).

[14] J. Sperling, W. Vogel, and G. S. Agarwal, "True photocounting statistics of multiple on-off detectors," Phys. Rev. A **85**, 023820 (2012).

[15] M. Jönsson and G. Björk, "Evaluating the performance of photon-number-resolving detectors," Phys. Rev. A **99**, 043822 (2019).

[16] C. Cahall, K. L. Nicolich, N. T. Islam, G. P. Lafyatis, A. J. Miller, D. J. Gauthier, and J. Kim, "Multi-photon detection using a conventional superconducting nanowire single-photon detector," Optica **4**, 1534 (2017).

[17] D. Zhu, M. Colangelo, C. Chen, B. A. Korzh, F. N. C. Wong, M. D. Shaw, and K. K. Berggren, "Resolving photon numbers using a superconducting nanowire with impedance-matching taper," Nano Lett. **20**, 3858 (2020).

[18] M. Endo, T. Sonoyama, M. Matsuyama, F. Okamoto, S. Miki, M. Yabuno, F. China, H. Terai, and A. Furusawa, "Quantum detector tomography of a superconducting nanostrip photon-number-resolving detector," Opt. Express **29**, 11728 (2021).

[19] S. Sempere-Llagostera, G. S. Thekkadath, R. B. Patel, W. S. Kolthammer, and I. A. Walmsley, "Reducing $g^{(2)}(0)$ of a parametric down-conversion source via photon-number resolution with superconducting nanowire detectors," Opt. Express **30**, 3138 (2022).

[20] S. I. Davis, A. Mueller, R. Valivarthi, N. Lauk, L. Narvaez, B. Korzh, A. D. Beyer, O. Cerri, M. Colangelo, K. K. Berggren, M. D. Shaw, S. Xie, N. Sinclair, and M. Spiropulu, "Improved heralded single-photon source with a photon-number-resolving superconducting nanowire detector," Phys. Rev. Appl. **18**, 064007 (2022).

[21] G. Sauer, M. Kolarczik, R. Gomez, J. Conrad, and F. Steinlechner, "Resolving photon numbers using ultra-high-resolution timing of a single low-jitter superconducting nanowire detector," arXiv:2310.12472 [quant-ph] (2023).

[22] T. Schapeler, N. Lamberty, T. Hummel, F. Schlue, M. Stefszky, B. Brecht, C. Silberhorn, and T. J. Bartley, "Electrical trace analysis of superconducting nanowire photon-number-resolving detectors," Phys. Rev. Appl. **22**, 014024 (2024).

[23] L.-D. Kong, T.-Z. Zhang, X.-Y. Liu, H. Li, Z. Wang, X.-M. Xie, and L.-X. You, "Large-inductance superconducting microstrip photon detector enabling 10 photon-number resolution," Adv. Photonics **6**, 16004 (2024).

[24] J. W. N. Los, M. Sidorova, B. Lopez-Rodriguez, P. Qualm, J. Chang, S. Steinhauer, V. Zwiller, and I. E. Zadeh, "High-performance photon number resolving detectors for 850–950 nm wavelength range," APL Photonics **9**, 066101 (2024).

[25] S. Slussarenko and G. J. Pryde, "Photonic quantum information processing: A concise review," Appl. Phys. Rev. **6**, 041303 (2019).

[26] D. Y. Vodolazov, "Minimal timing jitter in superconducting nanowire single-photon detectors," Phys. Rev. Appl. **11**, 014016 (2019).

[27] J. P. Allmaras, A. G. Kozorezov, B. A. Korzh, K. K. Berggren, and M. D. Shaw, "Intrinsic timing jitter and latency in superconducting nanowire single-photon detectors," Phys. Rev. Appl. **11**, 034062 (2019).

[28] D. Y. Vodolazov, "Single-photon detection by a dirty current-carrying superconducting strip based on the kinetic-equation approach," Phys. Rev. Appl. **7**, 034014 (2017).

[29] M. Sidorova, A. Semenov, H.-W. Hübers, I. Charaev, A. Kuzmin, S. Doerner, and M. Siegel, "Physical mechanisms of timing jitter in photon detection by current-carrying superconducting nanowires," Phys. Rev. B **96**, 184504 (2017).

[30] A. D. Semenov, M. Sidorova, M. A. Skvortsov, A. Kuzmin, K. Ilin, and M. Siegel, "Local thermal fluctuations in current-carrying superconducting nanowires," Phys. Rev. B **102**, 184508 (2020).

[31] A. G. Kozorezov, C. Lambert, F. Marsili, M. J. Stevens, V. B. Verma, J. P. Allmaras, M. D. Shaw, R. P. Mirin, and S. W. Nam, "Fano fluctuations in

superconducting-nanowire single-photon detectors," Phys. Rev. B **96**, 054507 (2017).
[32]C. Carbillet, V. Cherkez, M. A. Skvortsov, M. Feigel'Man, F. Debontridder, L. B. Ioffe, V. S. Stolyarov, K. Ilin, M. Siegel, D. Roditchev *et al.*, "Spectroscopic evidence for strong correlations between local superconducting gap and local Altshuler-Aronov density of states suppression in ultrathin NbN films," Phys. Rev. B **102**, 024504 (2020).
[33]H. Wu, C. Gu, Y. Cheng, and X. Hu, "Vortex-crossing-induced timing jitter of superconducting nanowire single-photon detectors," Appl. Phys. Lett. **111**, 062603 (2017).
[34]D. Y. Vodolazov, N. N. Manova, Y. P. Korneeva, and A. A. Korneev, "Timing jitter in NbN superconducting microstrip single-photon detector," Phys. Rev. Appl. **14**, 044041 (2020).
[35]A. Lipton and V. Kaushansky, "On the first hitting time density of an Ornstein-Uhlenbeck process," arXiv:1810.02390 [q-fin.CP] (2018).
[36]K. L. Nicolich, C. Cahall, N. T. Islam, G. P. Lafyatis, J. Kim, A. J. Miller, and D. J. Gauthier, "Universal model for the turn-on dynamics of superconducting nanowire single-photon detectors," Phys. Rev. Appl. **12**, 034020 (2019).
[37]M. Sidorova, A. Semenov, H.-W. Hübers, A. Kuzmin, S. Doerner, K. Ilin, M. Siegel, I. Charaev, and D. Vodolazov, "Timing jitter in photon detection by straight superconducting nanowires: Effect of magnetic field and photon flux," Phys. Rev. B **98**, 134504 (2018).
[38]B. Korzh, Q.-Y. Zhao, J. P. Allmaras, S. Frasca, T. M. Autry, E. A. Bersin, A. D. Beyer, R. M. Briggs, B. Bumble, M. Colangelo *et al.*, "Demonstration of sub-3 ps temporal resolution with a superconducting nanowire single-photon detector," Nat. Photonics **14**, 250 (2020).
[39]M. Sidorova, A. D. Semenov, H.-W. Hübers, S. Gyger, S. Steinhauer, X. Zhang, and A. Schilling, "Magnetoconductance and photoresponse properties of disordered NbTiN films," Phys. Rev. B **104**, 184514 (2021).
[40]M. V. Sidorova, A. G. Kozorezov, A. V. Semenov, Y. P. Korneeva, M. Y. Mikhailov, A. Y. Devizenko, A. A. Korneev, G. M. Chulkova, and G. N. Goltsman, "Nonbolometric bottleneck in electron-phonon relaxation in ultrathin WSi films," Phys. Rev. B **97**, 184512 (2018).
[41]R. Jaha, C. A. Graham-Scott, A. S. Abazi, W. Pernice, C. Schuck, and S. Ferrari, "Kinetic inductance and jitter dependence of the intrinsic photon number resolution in superconducting nanowire single-photon detectors," arXiv:2410.23162 [quant-ph] (2024).
[42]J. J. Renema, G. Frucci, Z. Zhou, F. Mattioli, A. Gaggero, R. Leoni, M. J. A. de Dood, A. Fiore, and M. P. van Exter, "Modified detector tomography technique applied to a superconducting multiphoton nanodetector," Opt. Express **20**, 2806 (2012).
[43]M. Sidorova, A. D. Semenov, H.-W. Hübers, S. Gyger, and S. Steinhauer, "Phonon heat capacity and self-heating normal domains in NbTiN nanostrips," Supercond. Sci. Technol. **35**, 105005 (2022).
[44]D. F. Santavicca, J. K. Adams, L. E. Grant, A. N. McCaughan, and K. K. Berggren, "Microwave dynamics of high aspect ratio superconducting nanowires studied using self-resonance," J. Appl. Phys. **119**, 234302 (2016).
[45]N. Calandri, Q.-Y. Zhao, D. Zhu, A. Dane, and K. K. Berggren, "Superconducting nanowire detector jitter limited by detector geometry," Appl. Phys. Lett. **109**, 152601 (2016).
[46]A. Kuzmin, S. Doerner, M. Sidorova, S. Wuensch, K. Ilin, M. Siegel, and A. Semenov, "Geometrical jitter and bolometric regime in photon detection by straight superconducting nanowire," IEEE Trans. Appl. Supercond. **29**, 2201105 (2019).
[47]M. Colangelo, B. Korzh, J. P. Allmaras, A. D. Beyer, A. S. Mueller, R. M. Briggs, B. Bumble, M. Runyan, M. J. Stevens, A. N. McCaughan *et al.*, "Impedance-matched differential superconducting nanowire detectors," Phys. Rev. Appl. **19**, 044093 (2023).
[48]A. Mueller, E. E. Wollman, B. Korzh, A. D. Beyer, L. Narvaez, R. Rogalin, M. Spiropulu, and M. D. Shaw, "Time-walk and jitter correction in SNSPDs at high count rates," Appl. Phys. Lett. **122**, 044001 (2023).
[49]C. Schuck, "Quantum sensing with waveguide-integrated superconducting nanowire single photon detectors," presented at International Conference "Quantum sensing," Paris, France, 4–6 June 2024.
[50]J. K. W. Yang, A. J. Kerman, E. A. Dauler, V. Anant, K. M. Rosfjord, and K. K. Berggren, "Modeling the electrical and thermal response of superconducting nanowire single-photon detectors," IEEE Trans. Appl. Supercond. **17**, 581 (2007).
[51]M. Sidorova, A. D. Semenov, A. Zaccone, I. Charaev, M. Gonzalez, A. Schilling, S. Gyger, and S. Steinhauer, "Low-temperature heat transport under phonon confinement in nanostructures," Phys. Rev. B **110**, 134513 (2024).
[52]X. Zhang, A. Engel, Q. Wang, A. Schilling, A. Semenov, M. Sidorova, H.-W. Hübers, I. Charaev, K. Ilin, and M. Siegel, "Characteristics of superconducting tungsten silicide W_xSi_{1-x} for single photon detection," Phys. Rev. B **94**, 174509 (2016).
[53]Y. P. Korneeva, D. Y. Vodolazov, A. V. Semenov, I. N. Florya, N. Simonov, E. Baeva, A. A. Korneev, G. N. Goltsman, and T. M. Klapwijk, "Optical single-photon detection in micrometer-scale NbN bridges," Phys. Rev. Appl. **9**, 064037 (2018).
[54]I. Charaev, Y. Morimoto, A. Dane, A. Agarwal, M. Colangelo, and K. K. Berggren, "Large-area microwire MoSi single-photon detectors at 1550 nm wavelength," Appl. Phys. Lett. **116**, 242603 (2020).
[55]J. Chiles, S. M. Buckley, A. Lita, V. B. Verma, J. Allmaras, B. Korzh, M. D. Shaw, J. M. Shainline, R. P. Mirin, and S. W. Nam, "Superconducting microwire detectors based on WSi with single-photon sensitivity in the near-infrared," Appl. Phys. Lett. **116**, 242602 (2020).
[56]A. S. Abazi, R. Jaha, C. A. Graham-Scott, W. H. P. Pernice, and C. Schuck, "Multi-photon enhanced resolution for superconducting nanowire single-photon detector-based time-of-flight lidar systems," Phys. Rev. Res. **7**, 033114 (2025).
[57]A. Pearlman, A. Cross, W. Slysz, J. Zhang, A. Verevkin, M. Currie, A. Korneev, P. Kouminov, K. Smirnov, B. Voronov *et al.*, "Gigahertz counting rates of NbN single-photon detectors for quantum communications," IEEE Trans. Appl. Supercond. **15**, 579 (2005).
[58]D. Zhu, M. Colangelo, B. A. Korzh, Q.-Y. Zhao, S. Frasca, A. E. Dane, A. E. Velasco, A. D. Beyer, J. P. Allmaras, E. Ramirez, W. J. Strickland, D. F. Santavicca, M. D. Shaw, and K. K. Berggren, "Superconducting nanowire single-photon detector with integrated impedance-matching taper," Appl. Phys. Lett. **114**, 042601 (2019).